EXPERIMENTAL INVESTIGATION OF DISSIMILAR ALUMINIUM ALLOY ON FRICTION STIR WELDING USING ANOVA [a]M. VAIRAVEL, [b]R. PUGAZHENTHI

[a] Research scholar, department of mechanical engineering, Vels institute of science, technology & advanced studies (vistas). chennai-117.
[b] Professor, Department Of Mechanical Engineering, Vels Institute Of Science, Technology & Advanced Studies (Vistas) Chennai- 117.

Abstract

FSW is a relatively hybrid technology in the joint, having been developed and patented by the UK standards of Welding Institute in the early 1990s. It is a derivation of the traditional approach that aims to provide considerable quality for But-joints and other joints. The current FWS technology is regarded as a unique approach, as it is carried out utilising classic fusion welding process. The current technology is mostly used for Aluminium Alloy -involved welding in the automotive, aerospace and shipping to other industries. In this paper find the results in mathematical modelling compared with experimental of the FSW process in dissimilar material effects on aluminium alloy welds is evaluation in the ANOVA regression mode. The present scenario in Analysis of Variance (ANOVA) was used to determine the relative impact of each factor and group of variables getting the predicted results. The following findings can be deduced from the current research: The welded zone's tensile strength, Micro hardness, Ultimate tensile strength, Yield strength found in this machine ASME standards condition to take the results to compared with the ANOVA. Using design analysis of experiments methodologies, And Process flow in dissimilar materials discusses and investigation of the hybrid values obtained in optimal factors associate connected with in

response of Characterization and stastical evaluation values getting the process parameters found and successful done it our research paper.

Keywords: Friction Stir Welding, Analysis of Variance, Velocity, Rotational Speed, Elongation, Yield Strength.

1 Introduction

FSW process is a brand-new solid-state welding method. Wayne Thomas developed and patented it in TWI, Great Britain, in December 1991. In this welding process, materials to be combined are re-solidified and melted. There is no separate melting of materials. The FSW functions on the principle i.e. severe metal deformation. So the defect free welding can be obtained. A solid-state joining takes place through heat produced by friction at the interface and a stirring action causing the material to flow. By applying the compressive forces, the prerequisite heat input is given in-between the joint of the material. 80 percent of the melting temperature of the components was used to connect them. FSW is made up of a non-consumable spinning tool with a shoulder and a pin that is specially developed. This tool is inserted between two plates that need to be joined. Following this, the rotating tool is longitudinally moved along the line of joining the materials.

The work plates, which are to be combined, are very tightly clamped by using a specifically designed fixture. All the degrees of freedom of movement of the work pieces are arrested to avoid the faces of abutting joints from separation. The pin length is designed somewhat lesser than the thickness of the work plates. The tool is pushed towards the workpieces and comes to a halt when the tool's shoulder comes into contact with the workpiece's surface. When applying downward axial force, the tool's shoulder must be in tight contact with the work surface. The function of the tool shoulder is to produce enough heat locally among the tool and the workpiece by friction. The tool pin's function is stirring the material for easy flow of the material to produce the joint. The material becomes more flexible by localising the heating around the pin, and the combination of rotating and translating the toolleads the material to migrate from the top to the rear of the pin. In addition to setting the plasticized metal in motion, the forging tool also adds substantial force to the metal behind it.

The shape, size and tool of the material play a complex role in the movement of the material around the pin (Boz and Kurt 2004). In the solid properties of a material, plastic deformation occurs between the workpieces, i.e. the dynamic re-crystallization. So the movement of the tool along the workpieces' weld interface makes the desired welding joint.

Fig. 1 Shows Schematic representation of FSW process

To join many commercial aluminium alloys for similar and dissimilar materials, FSW is a very suitable and successful process. Also the schematic representation of the friction stir welding process was illustrated in Figure 1.

Ahmed et.al [2020] recommended that the progression of material in FSW was the shoulder-driven stream and the pin-driven stream. In these sorts of streams, blend to shape a firm jointly and leave a pin width opening toward the finish of the cycle. In the FSW cycle, the tool moves toward the pin and the medium will be moved to the other edge of the pin from the main edge of the pin through the blending activity. Asmare et.al [2020] The apparatus shoulder activity separates the oxides on the faying surfaces which helps in spotless and firm holding of the materials. The functioning temperature of the FSW will consistently be 0.6 to 0.9 occasions the liquefying temperature of the materials to be welded. This strategy can be applied to deliver corner, butt, lap, spot, T, and filet joints.

Chanakyan, C., et al[2020] proposed a system utilizing DS-FSW which is double-side grating mix welding of 6061-T6. The thickness of the material was around six millimeters and they were acclimated to various thicknesses. The deliberate examination of this cycle was finished by dissecting the microstructural advancement at the hour of material rolling.

Das et.al [2020] investigated grating mix welded (FSW) 6061-T6 aluminum mixture microstructure and mechanical progression. The effects of indent regions on impact and shortcoming break improvement (FGC) were inspected.

Ugrasen, et.al [2018] proposed that the grain size, hardness, influence engaging energy, and hardness of a weld lump zone (WNZ) were more unassuming than those of a base material and warmth impacted zone.

A study by Ishraq et.al [2019] explored how welding processes affect the microstructural behavior, intermetallic phase distributions, and mechanical behavior of weld metals. Because friction stir welding is more expressive of microstructural changes than hot fusion welding, the longer temperature-time under high temperature, the longer interaction times between the base materials, and the larger area under plastic deformation, the changes were often more obvious. A high degree of interaction during the welding process will result in joints that have very poor mechanical integrity for easily brittle alloys.

Maneiah et.al [2020] explored the impact of hardware pin width and its stature and the shoulder breadths on grating mix welding mechanics, macro-structural properties, and warm properties. Besides, the impact of welding device boundaries including pin width and shoulder stature and nail tallness to the temperature of welding AA5083 combination just as pivotal and cross-over powers were examined. Toward the end, the ideal distances across the shoulder, pin stature, and pin are not settled.

In Mishra et.al [2019], property characteristics of a modern HSS were evaluated according to peak temperatures and cooling rates of the FSW. Using FSW, a thermo-mechanical HSS, produced by a controlled process, was welded with peak temperatures measured within the process zone ranging between about 900 and 650 °C.

Osman et.al [2019] examined the connection between twinning action, neighborhood textural variety, and crack conduct in twisting tests utilizing the Schmid factor investigation. Sivam et.al [2018] It has been shown that the impact of textural minor departure from crack conduct in bowing relies vigorously upon the nearby pressure state, which is very much clarified by the determined Schmid factor dependent on the expected pressure state for twisting. A nearby surface can be custom-made to work on joint strength and adjust crack conduct in FSW Mg welds.

Prasad et.al [2018] analyzed the impact of equipment shoulder estimation, rotational speed, welding speed, and critical weight as normal limits of the FSW communication in AA 8011. A demonstrative plan of investigations was aimed at ideal limits to support the assessment, and this achieved extraordinary comprehension among expected and preliminary data. For the arrangement of FSW of AA 8011, the dim social examination was applied to redesign the weld limits for multi-execution power usage, microhardness, and flexibility. The examination was driven using a Taguchi even group L9.

Rajendran et.al [2019] researched the grease impact of toughened Fe78Si9B13 glass particles in the FSW cycle of the metal AA6061and discovered the particles assumed a significant part through the improvement of the wear obstruction. Rathinasuriyan et.al [2020] This improvement in consumption and wear obstruction is an outcome of the decrease in grain size and the CTE confuse between the base metal and the built-up particles by FSP, and the oil impact of Fe78Si9B13 particles additionally adds to the upgraded erosion and wear opposition. Because of its interesting metastable construction, the FSP test with built-up particles in a shapeless state showed predominant consumption and wear opposition.

Senthil et.al [2020] directed a test in the helplessness of Aluminium-Copper-Lithium amalgam 2050 to erosion in Chloride arrangement in T34 and T84 conditions. They presumed that the weariness life of the T34 state was for the most part influenced by the weakness erosion. Express cyclic sales can be credited to expand engendering of inter-granular erosion.

Ugender, et.al [2018] In this study, temperatures were measured using thermocouples situated 5 to 10 mm from the joint line of the workpiece in the mid-thickness region. It appears that FSW allows welding of HSS in the inter-critical temperature range. Both at 40 °C and 60 °C, the best weld condition was 37% tougher than the best base material. It was about 70% efficient in terms of yield strength.

2. Selection of Materials

The wrought aluminum AA7075 is a part of the heat treatable 7xxx series. It comprises Aluminium, Copper, Magnesium, and Zinc as the major elements. The wrought aluminum material AA7075-T6 is available in roller plates with 6.35 mm thickness. Figure 2 displays the chemical composition of aluminium alloy.
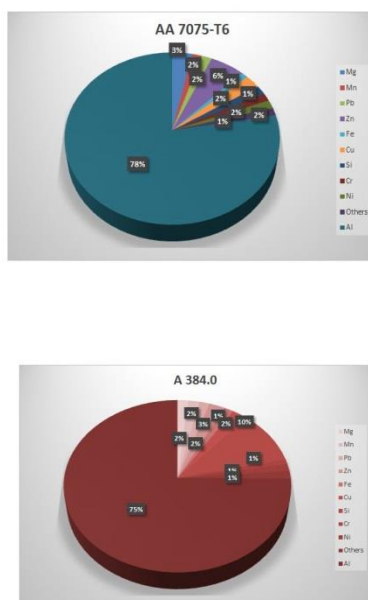

Figure 2 Chemical composition of A384.0-T6 and AA7075-T6

The cast aluminium A384.0-T6 is a part of the heat treatable 3xx.x series. It comprises Aluminium, Copper, Silicon, Magnesium, and Zinc as the major elements. Copper and Magnesium increase their strength and hardness, during as-cast temper and at elevated temperatures. The supplier provides A384.0-T6 as ingots that are machined to meet the required dimensions. The sides of the plates are ensured for parallelity. This is for proper clamping in the FSW fixture ensuring a uniform gap during the process of FSW. Table 1 show the chemical structure and mechanical characteristics of the AA7075-T6 and A384.0-T6 alloys.

Table 1 Aluminum alloy mechanical characteristics

Base Metals	AA 7075-T6	A 384.0
UTS (MPa)	597.2	102
YS (MPa)	389.7	-
Elongation (%)	13.87	1
Hardness (HRB)	92	35.8

2.1. Methods of Working
2.2.1 Flow process of FSW

Solid-state welding is referred to as FSW. It uses a different welding procedure to fuse high-strength Al alloys, which are notoriously hard to weld using standard methods. The FSW machine is illustrated in Figure 3. The process of friction stir welding is controlled with the spindle motor and the feed motor. Connected to the drive controllers are the spindle and the drive motors.

Figure 3 Friction stir welding machine

Mechanical gearboxes are used to boost the torque of the output shaft, spindle motor, and bed motor. The primary spindle motor is in charge of spindle rotation. The movement of all axes of the bed is powered by a feed bed motor. Emergency stop buttons and limit switches are provided for the safety of the operator and the work pieces and these are connected with the Peripheral Component Interconnect board. The work plates are butt joined. The work plates to be joined are tightly clamped by arresting all the movements. The specially designed fixture setup on the FSW machine is shown in Figure 2. FSW entails securely securing the to-be-welded work plates in a specifically constructed Friction Stir Welding fixture, preventing all dimensions of the working plates, and checking the welding quality. The machine investigated for this paper was R.V Machine tools from Coimbatore, India. It is one of India's most popular machines. This machine's model was FSW 3T NC. It was driven by a spindle taper ISO 40 and an 11KW/AC spindle motor. With the threaded hole, the table was 400mm X 350mm. Three axes were used to divide it. X, Y, and Z are their names. The thrust forces on the X and Y axes are 15 and 30 kilogrammes per square metre, respectively. The X, Y, and Z axis travel speeds ranged from 100mm to 300mm. The spindle noise ranged from 100 to 400mm. This machine was powered by a 22KVA generator. Steel, copper, and aluminium were employed as welding materials. However, a disimilar aluminium alloy was chosen in this instance.

2.2.2. Preparation of FSW Work pieces

Apart from the process parameters of tool rotation speed and welding speed, the success of the FSW is determined by the tool and work pieces design. The geometry of the tool and the material with which it is manufactured are both parts of the FSW Tool with work piece design.

Tool Design: The material to be utilized for tool manufacturing is HRC material with a hardness of 60 HRC. The tool pin is 60 mm long in total. The pin length and the diameter of the pin are 6 mm each. The shoulder diameter is 18 mm. The pin's shape is cylindrical. The geometry of the tool is shown in Figure 4.

Figure 4 Preparation of tool and work pieces' design

2.3 Methods of FSW-Working Characterization :
2.3.1 Tensile Analysis

The materials information are provided by the tensile test under the uniaxial tensile stresses on the strength, in terms of the UTS, ductility, and YS in terms of the percentage of elongation (% E). The tensile test specimens tested are shown in Figure 4. The two tensile specimens are prepared from the welded joint. To get the better accuracy of the test result, the specimens are cleaned with etchants. Universal testing equipment with a data collecting system is utilized to perform the tensile test. Fig. 5 illustrates the UTM.

Fig. 5 Universal Tensile testing machine with sample specimens

2.3.2 Microhardness Tester

The Microhardness tester is used to investigate the impact of ductile materials and grain reconfiguration on the mechanical characteristics of the weld nugget. To conduct the microhardness test, the test samples are prepared according to the ASTM-E384 standards. The prepared samples are tested by using Mitutoyo digital microhardness tester. This microhardness tester is shown in Figure 6.

Figure 6 Micro hardness tester

Based on a 1 mm increment, the measurements are taken from the mid thickness. The microhardness indentations of the recorded measurements are taken with the closest possible to the center of the thickness. The tests are conducted on the specimens applying a test load of 0.5 kg load for 10 seconds with a diamond indenter to make an indentation. The indentation mark is determined and the same was transformed into the hardness value. Vickers scales are made with a pyramid-shaped diamond indenter with a square base. The preparations of the samples are in the same way as preparing the sample of the microstructural specimens. The smooth

polished surfaces of the specimens provide a regular indentation shape which ensures the specimen is held perpendicular to the indenter to enable perfect measurements. To facilitate the test, the specimens are mounted in a plastic medium.

3.1 ANOVA Methods and process:

Using design of experiments methodologies, this papers discusses the investigation of the many process factors impacting the FSW process. It examines the connections between various FSW process factors and their impact on the FSW weld. The findings of the models are visually shown for better comprehension. The mathematical modelling of the FSW tool geometry effects on aluminium alloy welds is confirmed using the ANOVA regression model.

Results and Discussion

ANOVA is a statistical method that is used to test if the developed model is adequate. It's also used to assess the predicted model's quality and fit. An ANOVA test can be used to determine the importance of the convergent validity. The resulting models' R^2, adjusted R^2 (adj. R^2), and standard error (SE) are shown in Table 2.

Table 2 Experimental Vs predicted value of response

Runs	UTS		YS		% Elongation		Hardness (Hv)	
	Exp	Pre	Exp	Pre	Exp	Pre	Exp	Pre
1	252.80	251	197.18	196	1.1	1.60	130.0	127.35
2	272.96	272	212.91	212	2.5	2.65	142.5	143.58
3	260.22	258	201.97	200	1.7	2.20	144.0	141.31
4	255.85	257	199.56	200	2.3	2.58	124.0	126.74
5	246.33	248	192.14	193	1.0	1.25	121.0	121.95
6	267.80	267	208.88	208	2.2	2.64	155.0	154.01
7	261.76	264	204.17	206	2.8	2.91	141.5	142.83
8	248.06	247	193.49	192	1.0	1.33	115.0	113.97
9	260.60	262	203.27	196	1.2	2.00	138.0	141.10
10	277.37	275	215.35	214	3.0	3.52	140.6	139.14
11	264.02	265	205.94	215	2.6	2.71	141.0	142.63
12	252.37	252	196.85	197	1.4	1.74	118.0	119.09
13	271.67	271	211.90	204	2.2	3.15	129.0	126.19
14	260.94	263	203.53	205	2.3	2.58	122.0	124.19
15	248.31	248	193.68	201	1.3	1.63	129.0	127.66
16	271.00	272	211.38	212	2.5	2.65	144.0	143.58
17	271.90	272	212.08	212	2.4	2.65	144.0	143.58
18	272.00	272	212.16	212	2.5	2.65	143.5	143.58
19	272.10	272	212.24	212	2.5	2.65	144.0	143.58
20	271.80	272	212.00	212	2.4	2.65	143.5	143.58

Table 3 displays the contrast of R² and adjusted R² for responses. At the 95 percent confidence level, the projected F-ratio values are greater than the tabulated value. As a result, the models are suitable.

Table 3 Contrast of R² and adjusted R² for responses

Responses	S Value	R²	Adjusted R²
UTS	3.01724	89.73	85.69
YS	2.31448	89.39	86.95
% E	1.13117	87.83	85.88
Hv	3.40989	87.49	85.22

DF stands for Degrees of Freedom.

P value = The minimal significance level at which the data is significant.

F- Ratio = Mean Sum of Squares for regression / Mean Sum of Squares for Residual.

Figure 7 and Table 6 shows the experimental values of ANOVA for ultimate tensile strength.

Table 4 ANOVA for UTS

Source	DF	Squares total	Adjusted average square	F Value	P Value	Whether the model is adequate?
Regression	9	1753.03	194.781	47.87	0.000	
Linear	3	848.19	282.729	69.48	0.000	
Square	3	837.89	279.298	68.64	0.000	
Interaction	3	66.95	22.317	5.48	0.017	
Error that persists	10	40.69	4.069			YES
Inconsistency	5	38.72	7.744	19.64	0.003	
Pure blunder	6	2.97	1.394			
Total	20	1793.72				

Table 5 ANOVA for YS

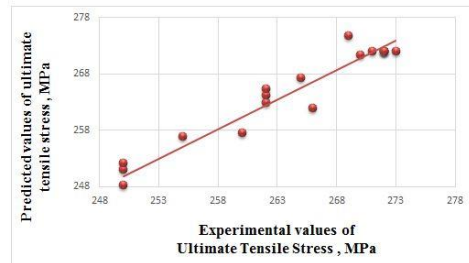| Source	DF	squares total	Adjusted average square	F Value	P Value	Whether the model is adequate?
Regression	9	1057.65	117.516	68.01	0.000	
Linear	3	499.80	166.600	96.42	0.000	
Square	3	522.82	174.272	100.86	0.000	
Interaction	3	35.03	11.676	6.76	0.009	
Error that persists	11	17.28	1.728			YES
Inconsistency	6	16.08	3.215	13.36	0.006	
Pure blunder	6	1.20	0.241			
Total	22	1074.92				

Fig 7 Scatter diagrams of experimental and predicted responses of regression model on UTS

Hypothesis tests are used in the choice process to make a choice. The p value is used in this test. This gives an indicator of the likelihood of incorrectly rejecting the Invalid theory if it is true.

The generated models are adequate based on this evidence. Scatter diagrams are used to evaluate the models' validity. Figure 8 and Table 5 shows the experimental values of ANOVA for yield strength.
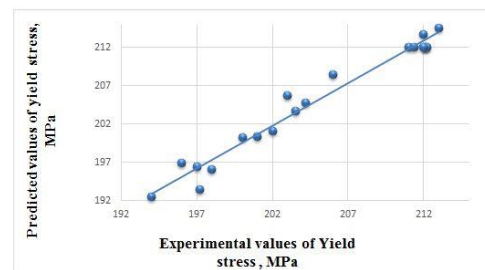

Fig 8 Scatter diagrams of experimental and predicted responses of regression model on YS

Figs 9 and Table 6 illustrates the experimental values of ANOVA for percentage of elongation The resulting result displays the experimental and anticipated responses of the process parameters.

Table 6 ANOVA for % of Elongation

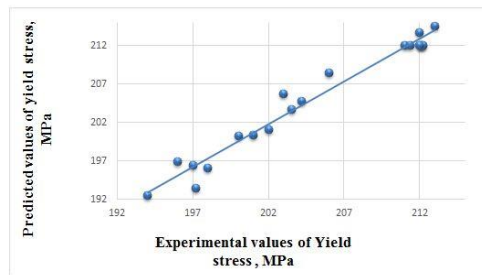| Source	DF	squares total	Adjusted Average square	F Value	P Value	Whether the model is adequate?
Regression	9	15.6341	1.73713	43.01	0.000	
Linear	3	3.0634	1.02114	25.29	0.000	
Square	3	7.8457	2.61524	64.76	0.000	
Interaction	3	4.7250	1.57500	39.00	0.000	YES
Residual error	11	1.4039	0.04039			
Lack of fit	6	1.4039	0.08077	*	*	
Pure error	6	1.0000	0.00000			
Total	22	16.0380				

Fig 9 Scatter diagrams of experimental and predicted responses of regression model on Percentage of elongation

Figure 10 and Table 7 shows the experimental values and predicted response of regression model of ANOVA for Hv.

These replies are evenly spaced around the 45-degree centre line. This demonstrates a perfect match for the empirical models that have been created.

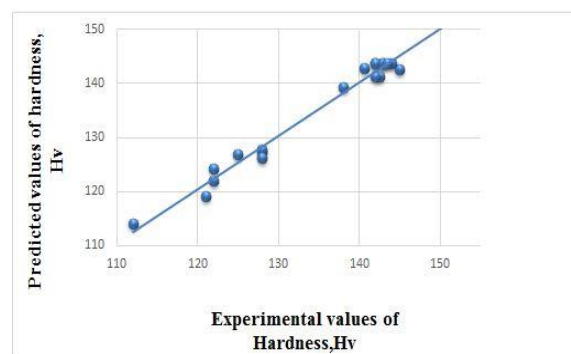| Cause	DF	squares total	Adjusted mean square	F Value	P Value	Whether the model is adequate?
Regression	9	2269.86	252.206	47.76	0.000	
Linear	3	1543.66	514.555	97.44	0.000	
Square	3	621.03	207.010	39.20	0.000	
Interaction	3	105.16	35.053	6.64	0.010	
Residual error	11	52.81	5.281			YES
Lack of fit	6	51.10	10.220	29.91	0.001	
Pure error	6	1.71	0.342			
Total	22	2322.66				

Table 7 ANOVA for Hv

Fig 10 Scatter diagrams of experimental and predicted responses of regression model on Hardness

The residuals are represented in a graphical form called a Residual plot. The vertical axis of the residual plot is used to plot residuals and the horizontal axis to plot independent variables. As the points on the horizontal axis of the residual plot graphs are distributed randomly, a linear regression model would be appropriate. Otherwise it is suitable for a non-linear model. A residual versus fit plot is the most commonly created plot when performing residual analysis. Plots are used to identify those features such as non-linearity, outliers and unequal variances in errors. The Histograms appear approximately symmetric and bell shaped. The residual versus observation plots verifies the assumptions that the residuals are uncorrelated with each other. Figure 11 shows the effects of tool rotation speed and welding speed for UTS
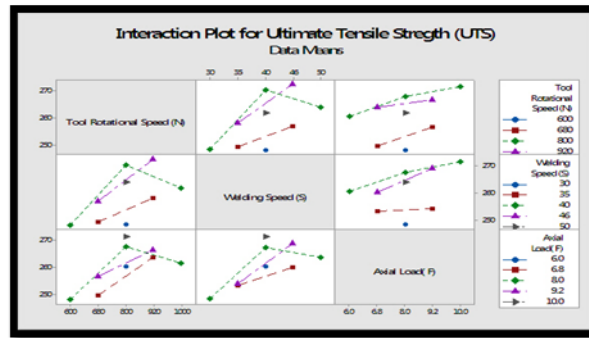
Figure 11 Effects of tool rotation speed and welding speed for UTS

The two-way interaction effects are the focus of this study. After accounting for fusing speed and rotor velocity, the remaining process parameter axial load is used to calculate the mean level. In the same way, the axial load and the welding speeds interaction are considered, the tool rotational speed is taken as the mean level. Table 8 and Figure 12 illustrates the combined effects of tool rotation speed and welding speed for yield strength.

Table 8 Combined effects of tool rotation speed and welding speed for YS

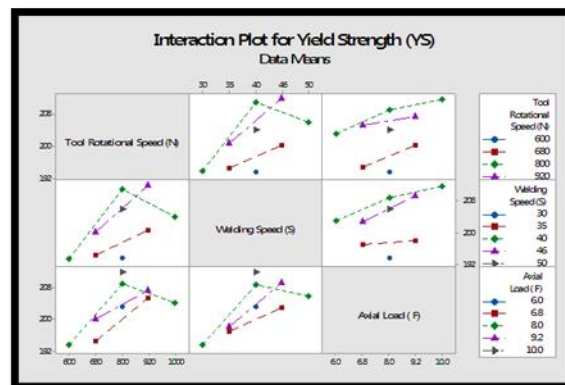| S.No	Rotational Velocity	Welding rate	Combined effect
1	Increases	Increases	Decreases
2	Increases	Decreases	Increases
3	Decreases	Rises	Sharp Decrease
4	Decreases	Drops	Little Decrease

Figure 12 effects of tool rotation speed and welding speed for YS

Fig 13 shows the Residual plots for Percentage of elongation. It shows that, A straight line is drawn from the residuals to the normal probability. The higher residual limit is +0.20 and the lower residual limit is -0.20. The fitted residual values have not given a clear model. At the zero level of the residual, the maximum frequency level is 8 shows in the histogram plot. The observed residual orders are within the limits. So it is proven that, to be adequate.
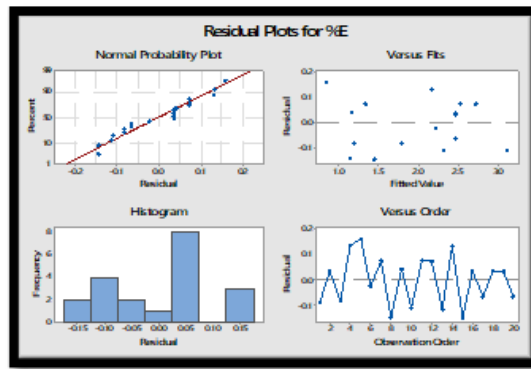
Fig 13 Residual plots for Percentage of elongation

This parameter identifies an input variable setting combination. This optimises a set of replies or a single response at the same time. The explanations of the heuristic plot for the input factors discovered for TS was clearly shown in Figs 14.
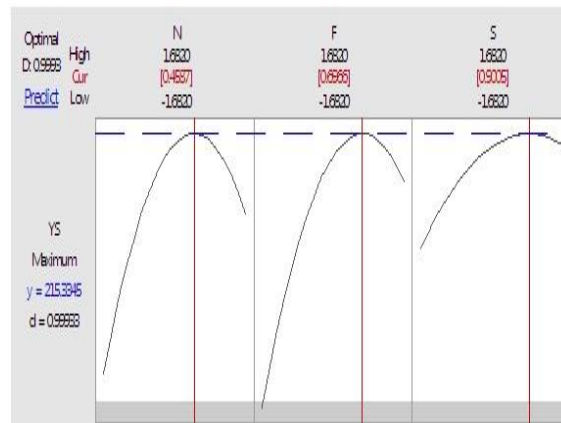

Fig 14 Optimization plot for tensile strength using response optimizer

Conclusions

These conclusions were drawn from DOE experiments.

i. FSW is feasible when the aluminium alloys AA 7075-T6 and A384.0-T6 are combined.

ii. The tool's rotating speed, axial load, and welding speed are all important process parameters that impact the joint's quality.

iii. At a 95% confidence level, the generated models were confirmed.

iv. At a particular level, increasing tool speed and axial load resulted in a greater response of UTS, YS, percent of E, and Hv. As each response reaches a maximum value, the value decreases.

v. Optimizing the process parameters will yield the best tensile strength characteristics and maximum hardness.

vi. In this research, the optimized process parameters are 920 rpm, an axial load of 9.2 kilo Newton and the welding speed of 46mm/min.

References:

1. Ahmed, Shuja, and Probir Saha. "Selection of optimal process parameters and assessment of its effect in micro-friction stir welding of AA6061-T6 sheets." *The International Journal of Advanced Manufacturing Technology* 106.7 (2020): 3045-3061.
2. Asmare, Assefa, Raheem Al-Sabur, and Eyob Messele. "Experimental Investigation of Friction Stir Welding on 6061-T6 Aluminum Alloy using Taguchi-Based GRA." *Metals* 10.11 (2020): 1480.

3. Chanakyan, C., et al. "Parametric optimization for friction stir welding with AA2024 and AA6061 aluminium alloys by ANOVA and GRG." *Materials Today: Proceedings* 27 (2020): 707-711.
4. Das, A. Daniel, S. N. Vijayan, and N. Subramani. "Investigation on welding strength of fsw samples using taguchi optimization technique." *Journal of Critical Reviews* 7.9 (2020): 179-182.
5. Ishraq, Muhammad Yasir, et al. "Analysing significant process parameters for friction stir welding of polymer composite." *The International Journal of Advanced Manufacturing Technology* 105.12 (2019): 4973-4987.
6. Maneiah, D., et al. "Process parameters optimization of friction stir welding for optimum tensile strength in Al 6061-T6 alloy butt welded joints." *Materials Today: Proceedings* 27 (2020): 904-908.
7. Mishra, R. S., and Preety Rani. "Experimental investigation of joining of aluminum alloy 5083 by Friction Stir Welding (FSW)." *International Journal of Research in Engineering and Innovation* 3.5 (2019): 306-309.
8. Osman, Nora, et al. "Effect of Process Parameters on Interfacial Bonding Properties of Aluminium–Copper Clad Sheet Processed by Multi-Pass Friction Stir-Welding Technique." *Metals* 9.11 (2019): 1159.
9. Prasad, MVR Durga, and Kiran kumar Namala. "Process parameters optimization in friction stir welding by ANOVA." *Materials Today: Proceedings* 5.2 (2018): 4824-4831.
10. Rajendran, C., et al. "Identifying combination of friction stir welding parameters to maximize strength of lap joints of AA2014-T6 aluminium alloy." *Australian Journal of Mechanical Engineering* 17.2 (2019): 64-75.
11. Rathinasuriyan, C., and VS Senthil Kumar. "Optimisation of submerged friction stir welding parameters of aluminium alloy using RSM and GRA." *Advances in Materials and Processing Technologies* (2020): 1-14.
12. Senthil, S. M., et al. "A multi-objective optimization of the friction stir welding process using RSM-based-desirability function approach for joining aluminum alloy 6063-T6 pipes." *Structural and Multidisciplinary Optimization* 62.3 (2020): 1117-1133.
13. Sivam, SP Sundar Singh, et al. "Grey relational analysis and anova to determine the optimum process parameters for friction stir welding of Ti and Mg alloys." *Periodica Polytechnica Mechanical Engineering* 62.4 (2018): 277-283.
14. Ugender, S. "Influence of tool pin profile and rotational speed on the formation of friction stir welding zone in AZ31 magnesium alloy." *Journal of magnesium and alloys* 6.2 (2018): 205-213.
15. Ugrasen, G., et al. "Optimization of process parameters for Al6061-Al7075 alloys in friction stir welding using Taguchi's technique." *Materials Today: Proceedings* 5.1 (2018): 3027-3035.